

# Measuring the dust opacity of the debris disk around HD 107146 with transit photometry

A. Uthor<sup>1</sup> and A. Uthor<sup>2</sup>,\*

<sup>1</sup> Institute1, University1, Address1  
 e-mail: e@mail1

<sup>2</sup> Institute2, University2, Address2  
 e-mail: e@mail2 \*\*

Received September 29, 2023; accepted Month day, year

## ABSTRACT

**Context.** Differential photometry has been essential for probing galactic structure and composition. Using a background object the opacity of interstellar dust can be determined using the Beer-Lambert law. This method can also be used to probe dusty debris disks, with the added benefit of being able to use transiting background objects that have been imaged before being extinguished by the disk. The relative motion of the HD 107146 disk and the Vermin galaxy has lead to the disk occulting the background galaxy starting in 2011. Three observation campaigns have imaged the occultation from 2004 until 2019.

**Aims.** We aim to use differential transit photometry to independently estimate the optical depth of dust in the HD 107146 debris disk using the Vermin galaxy as a background light source.

**Methods.** (Image processing/cleanup?) We use HST/STIS observations from 2011 to 2019 to build a surface brightness model of the disk. The model is then subtracted from the observations to remove the disk flux, which leaves only the extinguished galaxy in the image. Then we select one 2011 epoch as the reference observation. Assuming that the optical depth is proportional to the surface brightness of the dust, we find the optical depth and its posterior by minimizing the residual sum of squares of the  $\chi^2$  residuals of the extinguished galaxies and reference as a function of the optical depth and other nuisance parameters using a MCMC method.

**Results.** We find an upper limit on the optical depth of  $10^{-4} - 10^{-3}$  for the dust in the HD 107146 disk. This new limit is close to the detection limit of our method. Importantly, we have not needed to a-priory estimate a constant mean dust density in the disk and find a mean dust density of  $1.5 \pm 0.025 \text{ g cm}^{-3}$  and opacity of  $\approx 1.55 \times 10^{-18} \text{ cm}^2/\text{g}$  in the disk.

**Key words.** kw1 – kw2 – kw3

## 1. Introduction

The processes in debris disks are important for a significant part of the life of solar systems, specifically with regards to planet formation. Our understanding is based on observations, and increasingly on models of the physical processes themselves. These models rest on assumptions that are difficult to validate. Methods to probe disks, specifically at small particle sizes which give hints about the governing processes in discs such as collisional cascades, grain agglomeration and planetesimal formation are hence needed.

Previously, galactic astronomy was in a similar situation with regards to interstellar dust. It was widely assumed that (spiral) galaxies are semi-transparent to their own starlight, and thus must contain little dust. White & Keel (1992) and later James & Puxley (1993) for the first time used differential photometry to directly measure the optical depth of dust in occulting galaxy pairs. This method uses the extinction of background light through some foreground medium, e.g. interstellar dust, to find the optical depth of the medium according to the Beer-Lambert law, see Equation 1.

$$T = \frac{\Phi_{\nu,1}}{\Phi_{\nu,0}} = e^{-\tau_\nu} \quad (1)$$

where  $T$  is the transmittance,  $\Phi_{\nu,0}$ ,  $\Phi_{\nu,1}$  is the flux at frequency  $\nu$  before and after passing through the medium, respectively.  $\tau_\nu$  is the optical depth of the medium which can be expressed in terms of the medium's density  $\rho$ , opacity  $\kappa$ , optical path length  $l$  and surface density  $\Sigma$  as shown in Equation 2.

$$\tau_\nu = \int \rho \kappa_\nu dl = \kappa_\nu \Sigma \quad (2)$$

The optical depth for an occulting, opaque and extended foreground  $F$  and background  $G$  source is then given by Equation 3, where the second term separates the observations which is only possible if both models  $F'$  and  $B'$  are known. (White III et al. 2000)

$$e^{-\tau'} = \frac{\langle F + Be^{-\tau} \rangle - F'}{B'} \cong \frac{(F - F')}{B'} + \frac{B}{B'} e^{-\tau} \quad (3)$$

When using this method for galactic astronomy one major disadvantage is that the relative motion of the two galaxies is often not sufficient to fully image the unocculted background galaxy. This means that the galaxies have to partially overlap and the extinguished part of the background galaxy needs to be modeled based on the unocculted part or the extinction is measured using e.g. reference stars and/or HII regions.

Recently, van Sluijs et al. (2018) extended this method to circumstellar debris disks. Using observations by Ardila et al. (2004, 2005) as well as Schneider et al. (2014) they fit a galaxy

\* Just to show the usage of the elements in the author field

\*\* The university of heaven temporarily does not accept e-mails

model to the 2004 observations where the galaxy is at sufficiently large separations to be assumed unocculted with respect to the 2011 observations. The transmission, assuming perfect models, is then found using Equation 4.

$$T' = \frac{\langle D + Ge^{-\tau} \rangle - D'}{G'}, \quad (4)$$

where  $D, G$  and  $D', G'$  is the disk, galaxy, disk model and galaxy model respectively. While their method is insufficient for performing transit photometry, they find that using their method would be able to detect a  $\tau \approx \Delta\tau$  of 0.04 or more at one  $\sigma$  confidence with future observations. This rests on two assumptions: 1) the opacity for the 2004 epoch is small compared to later observations and 2) the disk has a sharp cutoff over the galaxy core ( $r < h$ ). While the initial assumption is most likely accurate the second one is not as can be simply seen from the disk model by Schneider?, discussed in section 4. There is a gradual change of optical depth due to disk depth over the galaxy which results in an imprint in the galaxy flux. This means two things for this work; 1) we use differential photometry based on different observation epochs, where we will get better results when the galaxies are at positions with large differences in optical depth and hence disk depths. 2) we need to have an accurate model of the disk where the values are approximately proportional to the optical depth, where better proportionality means more precise results.

## 2. Observations

Our images of HD 107146's debris disk and the background galaxy are from the HST and use a coronagraph as well as HD 120066 as a reference star for the point spread function. The observational parameters are shown in Table 1. The observations in this work used STIS 50CCD. The detector is sensitive from roughly 2000 to 11000 Å. During the observations the HST takes several images during each epoch while at 5 different roll angles w.r.t. the sight-line to HD 107146 to create a roll combined analysis image without the wedges of the coronagraph blocking parts of the field of view.

**Table 1.** Overview of the epochs after 2011 taken by the STIS/50CCD.

Placeholder	table
look at	guidelines

The reduced epochs are shown in ???. In the following we label the observations as Epoch 0 to 7 (EP1 – 7) in their chronological order.

Starting circa 2011, the nearly face-on HD 107146 circumstellar debris ring serendipitously began, and is now continuing, the transit ingress phase of its superposition over an angularly small but (with HST) spatially resolved background galaxy prior dubbed the Vermin galaxy. We advantageously exploited HD 107146's high-proper-motion trajectory w.r.t. the Vermin galaxy backlighting a small sectional slice of the host star's exoplanetary debris system to probe multiple sight-lines through the nearly face-on debris disk over time. Resulting differential photometric measures of and through the disk circa 2017-2019, in concert with reprocessing of earlier epoch archival "baseline" data (with the galaxy at the outer periphery of the disk), can provide independent extinction/optical depth constraints on the disk through which the galaxy is seen with coronagraphic starlight suppression and PSF subtraction.

Utilizing HSTs imaging spectrograph (STIS), multi-roll observations of HD 107146 and of a contemporaneously imaged color-matched PSF template (calibration) star HD 120066 ( $\Delta[B - V] = -0.04$ ) were obtained in coronagraphic mode at eight epochs (denoted 0 – 7 in Table 1). In this mode the STIS 50CCD (unfiltered) visible-light detector provides broadband spectral sensitivity in the range roughly 0.2 to 1.1  $\mu\text{m}$  with a pivot wavelength of 0.58  $\mu\text{m}$  and FWHM 0.43  $\mu\text{m}$  at a native image scale of 50.77 mas per pixel.<sup>1</sup>

The first two epochs of images (denoted 0 and 1 in Table 1), then unconcerned with the placement of the Vermin galaxy. These were obtained using both occulting wedges A-1.0 and A-0.6 in HST GO program 12228 optimized for the needs of that program as discussed by Schneider et al. (2014) wherein first STIS images of HD 107146 were obtained. Subsequently, follow-on observations (denoted epochs 2-7) during transit ingress discussed herein were acquired using occulting wedge A-1.0 only with (all identical) exposures optimized for the anticipated disk+galaxy surface brightness as informed by the pathfinding GO 12228 observations.<sup>2</sup> These follow-on observations were executed twice annually<sup>3</sup> at six epochs during the disk transit ingress phase; see Table 1. At each follow-on epoch HD 107146 was multiply imaged in each of four contemporaneous single-orbit visits with each visit at a different celestial field (spacecraft roll) orientation differing nominally<sup>4</sup> by 4° to improve (in later combination) imaging efficacy and fidelity. The total HD 107146 integration time at each follow-on epoch was approx. 8314 s comprised of 5 identical (other than in orientation angle) 479 s exposures in each of four orbits with also one HD 120066 calibration orbit per epoch contemporaneously interleaved.

## 3. Image Calibration & Reduction

To produce a highest fidelity analysis quality (AQ) calibrated image resulting from all data acquired from each epoch, we followed as closely as possible the precepts, procedures and processes for HST/STIS multi-roll combined PSF-template subtracted coronagraphy as discussed in Schneider et al. (2014), and specifically as described in Schneider et al. (2016) (§5) with enumeration as below to which we refer the reader for details. This includes:

1. Instrumental calibration of raw to FLT files with calstis with dark, bias, non-linearity corrections incorporating observation contemporaneous STScI/CDBS reference files.
2. Occulted target location (centration and coalignment) by the X marks the spot method.
3. Sub-pixel jitter correction (due to fail-down to single FGS guiding in some visits).
4. Transformation to visit-level, median combined, count-rate images.

<sup>1</sup> FWHM of the STIS 50CCD PSF is 72 mas, but critical (Nyquist  $Q = 2$ ) sampling is obtained in most pixels with multi-roll imaging; See Schneider et al. (2018), §3.

<sup>2</sup> For details of the exposure/observation plan see: <https://www.stsci.edu/hst/phase2-public/XXXXX.pro> with XXXXX = 12228, 14714, 15221, or 15501.

<sup>3</sup> With unequal cadence due to HST scheduling constraints.

<sup>4</sup> But constrained in field orientation to avoid obscuring the galaxy by the STIS occulting wedges and unapodized diffraction spikes requiring  $< 4^\circ$  orientation differentials in some intra-epochal visits.

5. PSF-template subtraction/residual minimization (with idp3 s/w<sup>5</sup>; Stobie & Ferro (2006)) utilizing analogously reduced PSF-template star images.
6. Inter-visit north up rotation to a common celestial frame and origin (with bicubic-sinc interpolation).
7. Generation of visit-level bad data exclusion masks: wedge-shadowed, diffraction-spoke polluted, wedge-edge saturated and other anomalous pixels or image regions.
8. Multi-roll masked-median image combination to AQ images.
9. Photometric transformation from instrumental count rates to physical surface brightness ( $1 \text{ count } s^{-1} \text{ pixel}^{-1}$ ) =  $177 \text{ microJy arcsec}^{-2} = 18.04 \text{ Vmag arcsec}^{-2}$ .

Results after steps 5 and 8 are illustrated in Figure GS01.

#### 4. Disk Scattered-light Image Modeling

Figure 2 shows the circumstellar light scattered by the HD 107146 debris disk superimposed upon the Vermin galaxy field at each of the eight observational epochs after stellar PSF-template subtraction removing (most of) the instrumentally diffracted and scattered starlight. To also remove the disk light from each image we apply (subtract) an observationally (not physically) informed azimuthally featureless scattered-light model of an annular disk as discussed by Schneider et al. (2016) (g6) to which the reader is referred for details. This surface brightness model, predicated on Schneider et al. (2006)

Is this the right Schneider et al. 2006?

, includes a Gaussian radial taper of scattering particles at its inner and outer edges, azimuthal modulation with Henyey-Greenstein scattering asymmetry (Henyey & Greenstein 1941),  $r^{-2}$  diminution of the stellar illumination, and is sensitive to the disk viewing geometry.

We closely follow, develop, and subtract an empirically derived best-fit disk surface brightness model in concert with the parametric prescription of Schneider et al. (2016), ibid. This approach was successfully used in HST GO program 13786 to identify asymmetrical sub-structures in several other ring-like debris disks<sup>6</sup> including HD 207129 and HD 202628.

We illustrate with two examples. First, in Figure 3 left panel, to provide a fully spatially sampled image of the disk, we linearly combine the two pre-transit disk images closely-spaced epochs 0 and 1 from the GO 12228 data (c.f., Schneider et al. (2014), Figure 27) with large intra-visit roll images (see Table 1). Second, in ?? illustrating disk-light rejection with (same) model subtraction with the HD 107146 debris ring superimposed upon in-transit galaxy in epoch 2 AQ image.

Mention float32 (f4) encoding for disk model?

#### 5. Method

From section 4, we assume that  $\int \rho dl$  along the line of sight varies with the radial separation from the star i.e.  $\frac{d}{dr} \tau_v \neq 0$  which is supported by surface density models of e.g. Krivov (2010). Assuming that the optical depth is proportional to the surface brightness of the disk, we rewrite Equation 1 to include the disk surface brightness  $\hat{D}'$ , yielding Equation 5. This is a good-first

<sup>5</sup> See <https://archive.stsci.edu/prepds/laplace/idp3.html>.

<sup>6</sup> Although, obviously, the galaxy is not intrinsic to the disk, the same disk-light rejection paradigm applies.

order assumption since a brighter part of the disk, assuming that the particles inside the disk are the same size and have the same optical properties, will have either a higher density or the line-of-sight through the disk will be longer.

$$T_{adj} = \frac{\Phi_{v,1}}{\Phi_{v,0}} = e^{-\tau_v \times \hat{D}'} \quad (5)$$

The epochs are then given by Equation 6.

$$I = \langle D + G \times T_{actual} \rangle \quad (6)$$

First we subtract the disk model to remove the scattered light from the central star;

$$I_G = \langle D + G \times T_{actual} \rangle - D'. \quad (7)$$

Since the galaxy is at different positions with respect to the disk in the epochs, translating the galaxy as-is would result in residuals that include the imprint of the different disk extinctions convolved with the galaxy flux. Hence, we divide by the estimated transmission field  $T'(\tau'_v; D')$  constructed by Equation 5 where we test a model optical depth  $\tau'_v$ . So that the model galaxy image  $G'$  is given by Equation 8.

$$G'(\tau'_v) \equiv \frac{\langle D + G \times T_{actual} \rangle - D'}{T'(\tau'_v)}. \quad (8)$$

This means that we do not need to assume that the extinction at any epoch is zero.

We then define the residuals  $R$  for a single epoch pair,  $EP_{ref}$  and  $EP_{target}$ , by Equation 9, where we affine translate the model galaxy image of the reference epoch to the position of the target epoch using bi-linear interpolation.

$$R = G'_{target} - \text{affine}(G'_{ref}, \Delta x, \Delta y), \quad (9)$$

This method finds an upper opacity limit down to  $\tau_v \approx 10^{-7} - 10^{-6}$ , for representative, noiseless model images constructed using Equation 6, when the offsets between the images are known.

In order to find the posterior probability distribution of the optical depth we use the  $\chi^2$ -residual as given in Equation 10.

$$\chi^2_{target} = \sum_{i=0}^M \left[ \frac{G'_{target} - \text{affine}(G'_{ref}, \Delta x, \Delta y)}{\sigma_{RMS}} \right]^2, \quad (10)$$

where  $M$  is the masked target galaxy region, and the RMS noise  $\sigma_{RMS}$  is assumed to be constant over the image.

This residual is well defined for all  $G'_{target} \neq G'_{ref}$ , so the residual-sum-of-squares (RSS) follows from the  $\chi^2$ -residuals. There are two options for fitting the optical depth:

1. Select one epoch as a reference and evaluate the other epochs against it, mirroring the configuration van Sluijs et al. (2018) proposed. This leads to fitting  $1 + 2(N_{EP} - 1)$  parameters:  $\tau$  and  $N_{EP} - 1$  pairs of  $\Delta x, \Delta y$  w.r.t. the reference epoch.
2. Fit using the whole set of combinations of 2 epochs from the  $N$  epochs. This means fitting  $1 + 2 \times \binom{N}{2}$  parameters, again the optical depth and  $N$  pairs of  $\Delta x, \Delta y$ .

In this work we proceed with option 2 in order to exploit the equivariance of the combinations and hence construct the RSS as shown in Equation 11.

$$RSS = \sum_{i=1}^{N_{EP}} \chi^2_{EP_i} \quad (11)$$

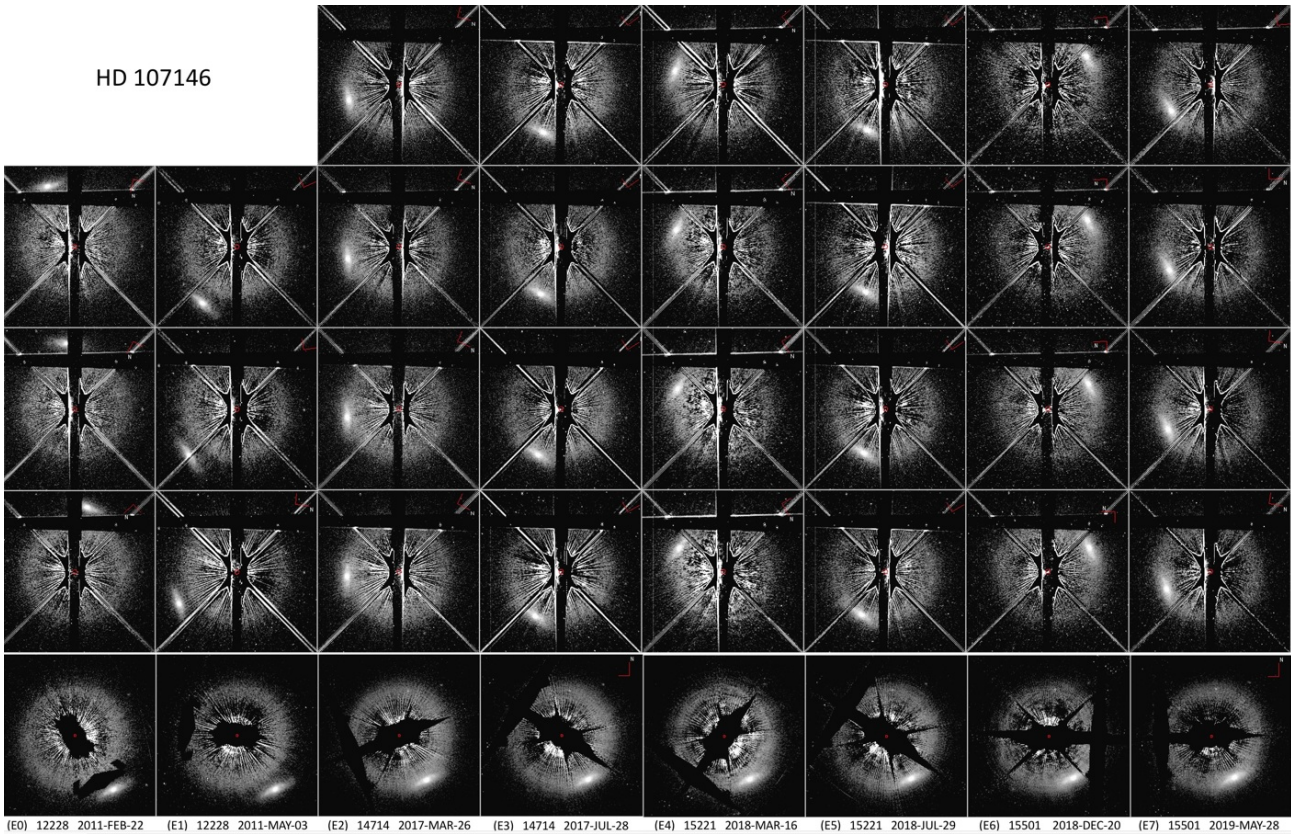


**Fig. 1.** Top four rows (incremental differential field orientations): Visit-level reductions after step 5 (PSF template subtraction) in Science Instrument Aperture Frame with rotationally invariant PSF and disk/galaxy co-rotating with telescope orientation. Bottom row: Epoch-level reductions after step 8 (multi-roll combination in north up (NUP) orientation). Central regions digitally masked as black are unsampled or degraded due to STIS occulting masks, HST diffraction spikes or other image/PSF-subtraction artifacts. Left to right columns: epoch 0 to epoch 7.

We derive posterior probability distributions and the Bayesian evidence with the nested sampling Monte Carlo algorithm MLFriends (Buchner 2016, 2019) using the UltraNest<sup>7</sup> package (Buchner 2021).

Mention prior space for dx, dy: linear for tau both log and linear

We verify our method by constructing representative model images based on Equation 6, with gaussian noise but without streaks or bad pixels. Experimentally, we find that our method is suitable to detect the optical depth of the dusty disk down to  $\tau_{min} \approx 10^{-4} - 5 \times 10^{-4}$ , and find that the residual  $R_i$  and  $\chi^2$ -residual images are suitable to visually inspect the goodness of the fit.

## 6. Results

### 6.1. Residual Images

The maximum likelihood point residual images, assuming a common opacity proportional to the disk brightness, are shown in Figure 4. Combinations with EP2 have a large residual pixel in the galaxy bulge which might be spurious noise or due to short lived processes within the bulge. A visual inspection of the corresponding pixel in EP2 does not seem corrupted and is very informative about the optical depth due to its high S/N it was not masked.

### 6.2. Optical Depth

We find an upper opacity limit (84<sup>th</sup> percentile) of  $\tau_{max} \leq 3.96 \times 10^{-4}$ . Figure 6 shows the  $\tau$  posterior probability distribution as well as the quantile functions for each of the  $\tau \times \sigma_D$  at the respective galaxy positions. For this plot we take  $\sigma_D$  as the mean disk SB in a 2 pixel radius around the inferred galaxy position.

## 7. Discussion

We detect upper limits for the optical depths around  $\tau_{max} = 1 \times 10^{-4} - 1 \times 10^{-3}$  depending on the extinction law used. This is reasonably close to the detection limit of us and Schneider et al. (2016). Nevertheless, our method is prone to underestimate the opacity slightly by having a small gradient towards lower optical depths and hence more walkers pile up near the physical limit than would otherwise. From experiments with representative model images this offset is small compared to  $\tau$  and other error sources.

### 7.1. Disk Mean Solid Particle Density

In previous work e.g. of Ricci et al. (2015) and van Sluijs et al. (2018) a uniform mean solid particle density was assumed in the disk. Both rely on probes of protoplanetary disks in the Taurus-Auriga star forming region. We avoid the implicit assumption that these PPDs are similar to the HD 107146 debris disk by deriving the mean solid density from the fractional luminosity  $f$ , the total effective cross section of the dust  $\sigma_{tot}$  and the dust mass  $M_{disk}$ .

<sup>7</sup> <https://johannesbuchner.github.io/UltraNest/>

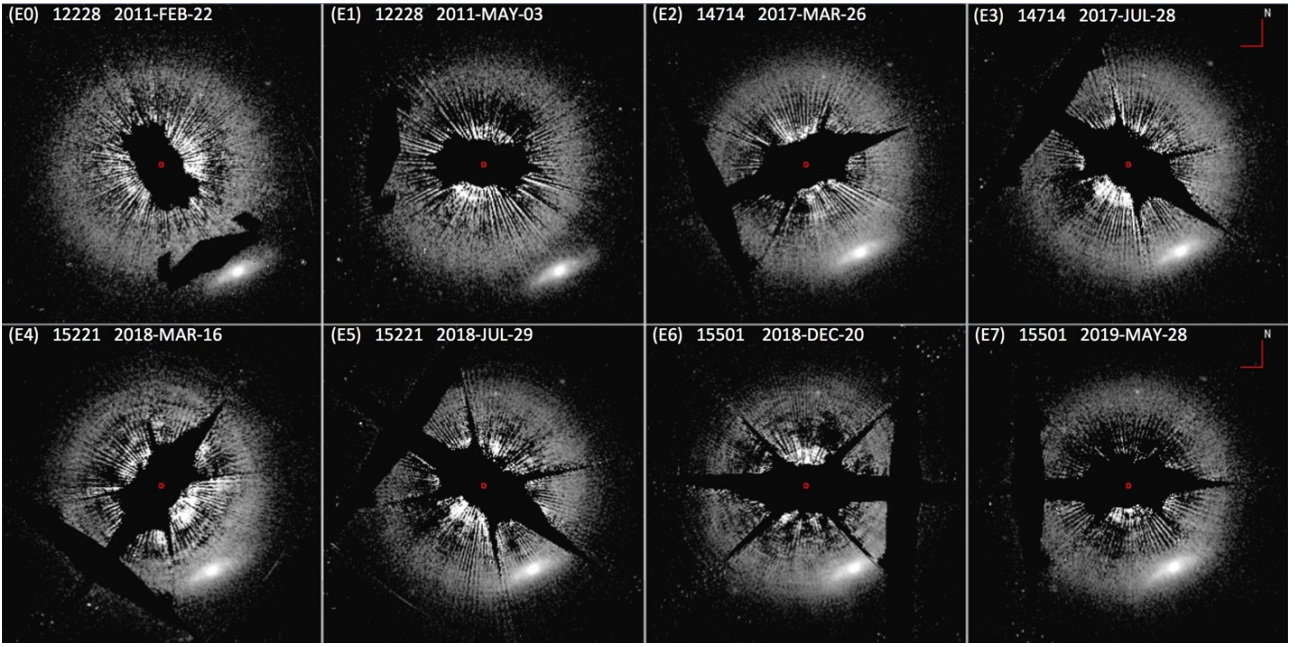


**Fig. 2.** HD107146 debris ring transit (ingress) over background galaxy - chronologically in panels E0 - E7. Same as Figure 1 bottom row (NUP) images, but illustrated in more detail. Panels E0/E1 epochs with galaxy located at pre-transit periphery of debris ring re-reduced from GO 12228. Other panels (starting ~6 years later) are twice a year with unequal cadence per HST scheduling constraints (assuring coronagraphically obscured regions do not superimpose on the location of the galaxy with other spacecraft orientations constraints). All images are astrometrically co-registered on the obscured central star (position indicated by small red dot), are shown as log10 stretch from [-2] to [-0.7] dex counts/sec/per pixel; north up, 300x300 pixel sub-array extracts centered on target. (1 pixel = 50.077 mas). FOVs extend further west than illustrated and provide a basis for background noise estimation. The vermin galaxy has a peak surface brightness (Gmax) of  $\sim 0.5$  counts/sec/per pixel, the disk at the same stellocentric angular distance with Dmax  $\sim 0.04$  counts/sec/pixel, and a background (at large distance from the star and galaxy with RMS noise  $\sigma_{rms} \approx 3 \times 10^{-3}$ .

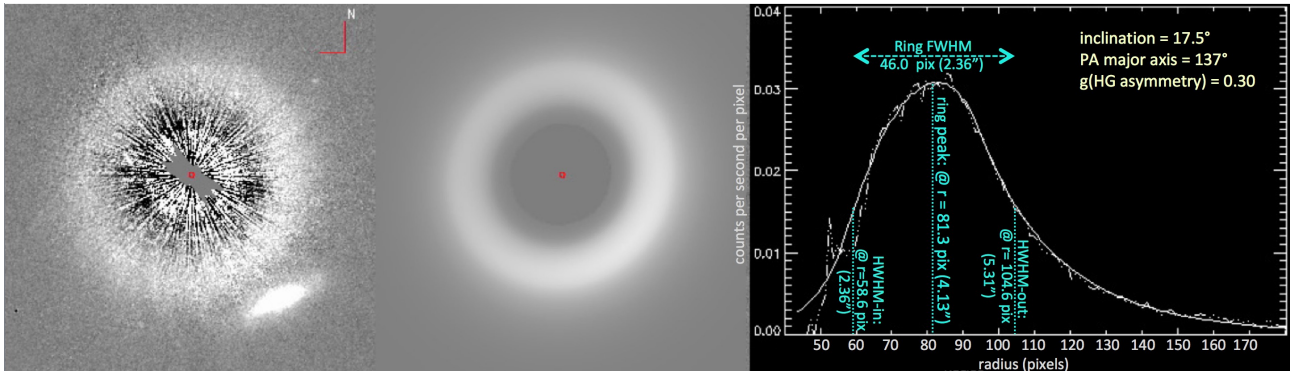


**Fig. 3.** Left: Epoch 0+1 AQ image of the HD 107146 debris ring fully sampled with the Vermin galaxy well separated beyond the periphery of the disk. Linear display range  $\pm 0.05$  counts per second per pixel to show the structure of remaining PSF-subtraction residuals without saturating at the radius of highest surface brightness while also revealing the low level of “pixel to pixel” noise in the sky background at the field boundaries. Middle: Model disk image at same display stretch derived from all eight epochs with galaxy masked. Right: Representative surface brightness radial profile/cross-section (arbitrarily along disk major axis) comparison of AQ image (solid line) vs. model comparison (dot-dashed line) showing excellent agreement at  $r > 65$  pixels (3.3'') in region of interest of galaxy reflex motion at epochs 0–7 inclusive.

Assuming a uniform dust distribution, the total cross section of the dust grains in the disk, assumed to be a torus of radius  $r_{disk}$  with a width of  $dr$  is given by:

$$\sigma_{tot} = 4\pi r_{disk}^2 f \quad (12)$$

with  $\sigma_{tot}$  to total cross section of the dust and  $f$  the fractional luminosity of the disk (Wyatt 2008). While Marino et al. (2018) take the outer radius of the disk from as  $135.6^{+1.1}_{-1.2}$  AU, and van Sluijs et al. (2018) assume an outer radius of  $\approx 180$  AU, the debris disk extends significantly further than that. This can be seen from scattered-light images which are sensitive to different dust sizes than IR observations (Ertel et al. 2011). van Sluijs

et al. (2018) estimate an extent of 200 – 250 AU. Taking a cut-off surface brightness of  $0.2 \text{ microJy arcsec}^{-2}$  for the furthest extend of the disk gives a stellocentric outer radius of  $\approx 9''$  or  $r_{disk, outer} = 240^{+10}_{-40}$  AU (Schneider et al. 2014). We take this estimate, rather than the previous values as the IR-flux at these larger radii still contribute to the fractional luminosity. The fractional luminosity was initially estimated by Moór et al. (2006) as  $9.2 \times 10^{-4} \pm 0.9 \times 10^{-4}$ , however Ertel et al. (2011) give a value of  $1.07 \times 10^{-3}$  and Schneider et al. (2014) of  $1.2 \times 10^{-3}$ . Since, Ertel et al. (2011) have multiple concerns about their

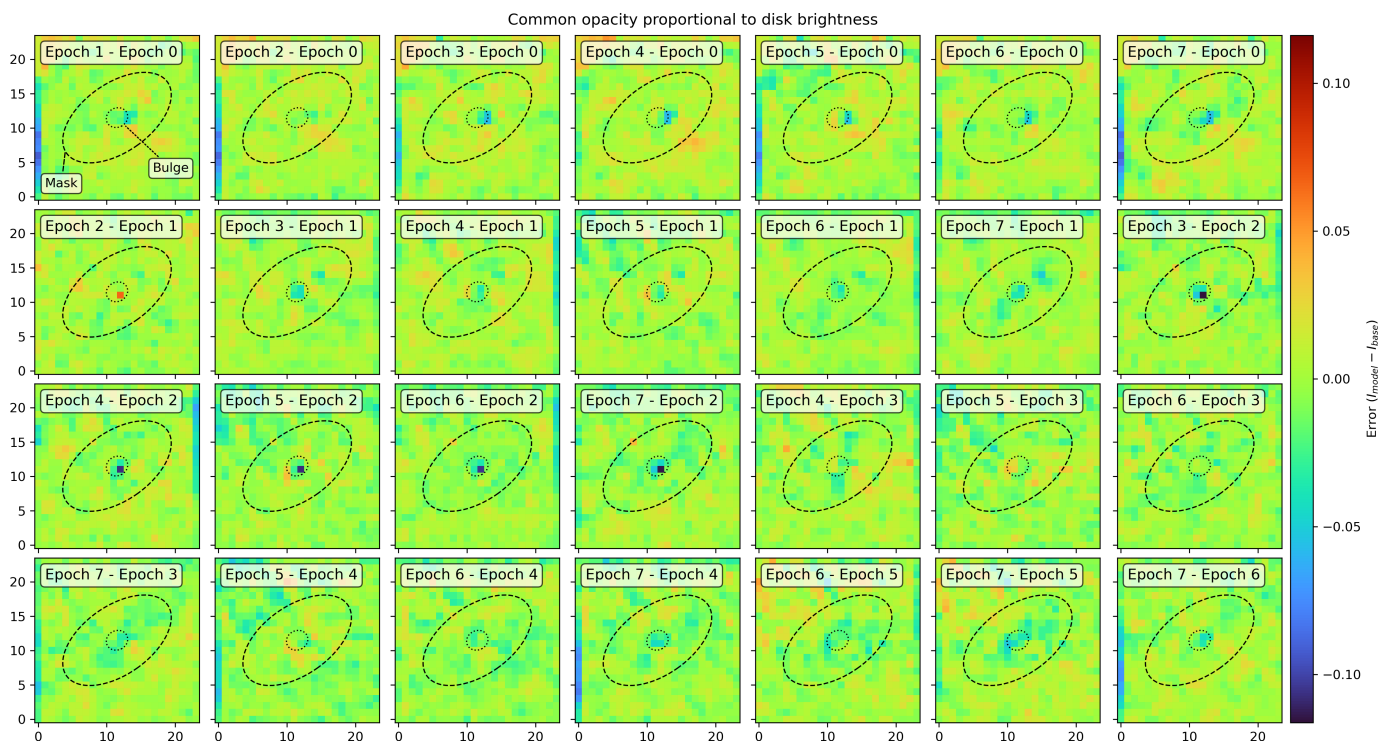


**Fig. 4.** Residuals at maximum likelihood point for all image pairs. The large residuals for pairs including EP2 are due to the specific pixel location of the galactic bulge with respect to the location of EP0 which is taken as the reference origin.

model (see their section 5.2) we will use the more recent value<sup>8</sup> from Schneider et al. (2014). The total cross section of the dust is then  $\sigma_{tot} = 860 \text{ AU}^2$ . We assume the dust in the debris disk is continually replenished, most likely by collisional cascades and grinding of planetesimals which continually (re-) produce  $\mu\text{m}$  size dust grains as suggested by Kenyon & Bromley (2005) in general and Ricci et al. (2015) for the HD 107146 disk. This is supported by the work of Chiang et al. (2009) who find, for the Formalhaut debris disk and grains produced by collisional cascades, a size of  $> 8 \mu\text{m}$ . Similar to van Sluijs et al. (2018), we assume the dust is mainly (astro-) silicate particles on circular orbits. The smallest grains are then continually blown out of the system by stellar radiation with a the minimum particle size - the blow-out grain size  $a_{min}$  - of  $2.7 \mu\text{m}$ . However, if the dust grains are not silicates the blow-out grain size could be as low as  $1.7 - 1.1 \mu\text{m}$  (Ricci et al. 2015; Marino et al. 2018). we will only consider the first case, as it is reasonable to assume that at least a large mass fraction of the dust is silicates according to Marino et al. (2018). In either case, we assume that the wavelength at which we probe the dust is much smaller than the blow-out grain size and hence we assume Mie scattering. The effective cross section of the (assumed spherical) dust grains is then given by Equation 13 and Equation 14.

$$\sigma_{grain} = 2\pi a^2 \quad (13)$$

$$\int_{a_{min}}^{\bar{a}} n(a') da' = \frac{1}{2} \quad (14)$$

with  $n(a)$  normalized as by van Sluijs et al. (2018).

<sup>8</sup> Note however, that the most recent work on the disk by Mesa et al. (2021) again use the value from Ertel et al. (2011).

Draine (2006) finds that solid particles growing by agglomeration in debris disks consisting of i.a. mainly silica, follow a power law size distribution  $dn/da \propto a^{-p}$ . Dohnanyi (1969); Tanaka et al. (1996) and Tanaka et al. (2005) show that this power law with  $3 \lesssim p \lesssim 3.5$ , under certain assumptions, is applicable to particles growing by coagulation and collisional fragmentation such as we expect for this debris disk. Weidenschilling (1997) argues that for the the solar nebula particles size can be approximated with  $p = 3.5$ . This power law is only valid for  $a \leq a_{max}$  and under the assumption that  $\lambda \leq a_{max}$  (Draine 2006) which we also required above. In the following we make the conservative assumption that  $a_{max} = 2 \text{ cm}$  from Ricci et al. (2015) following the work of van Sluijs et al. (2018). Ricci et al. (2015) find a grain size distribution for the disk of HD 107146 with  $p = 3.25 \pm 0.09$ . Recent work by Marino et al. (2018) also use a power law size distribution to model the debris disk of HD 107146, however, they assume  $3.36 \leq p \leq 3.5$  without further justification. In this work we will assume a size distribution as found by Ricci et al. (2015), i.e.  $p = 3.25 \pm 0.09$ . The average grain size is then  $\bar{a} = 3.7 \mu\text{m}$ .

The most accurate method to find the mass of a debris disk is through direct observation of the disk flux Alexander et al. (2014); Wyatt (2008). Using this method, Williams et al. (2004) find a lower limit for the dust mass of HD 107146s debris disk of  $M_{disk} = 0.10 \pm 0.02 M_{\oplus}$  by assuming a dust mass absorption coefficient. Without this assumption they set the limits for the dust mass to  $0.10 \leq M_{disk} \leq 0.43$  in  $M_{\oplus}$ . More recent investigations of the dust mass rely on fitting a disk model to observations. Ricci et al. (2015) find a disk mass of  $\approx 0.2 M_{\oplus}$ , wheres Marino et al. (2018) find a best fit value of  $0.250 \pm 0.004 M_{\oplus}$ . The difference in accuracy between the first and more recent estimations is mostly due to the different observatory capabilities, the James Clerk Maxwell Telescope and ALMA respec-

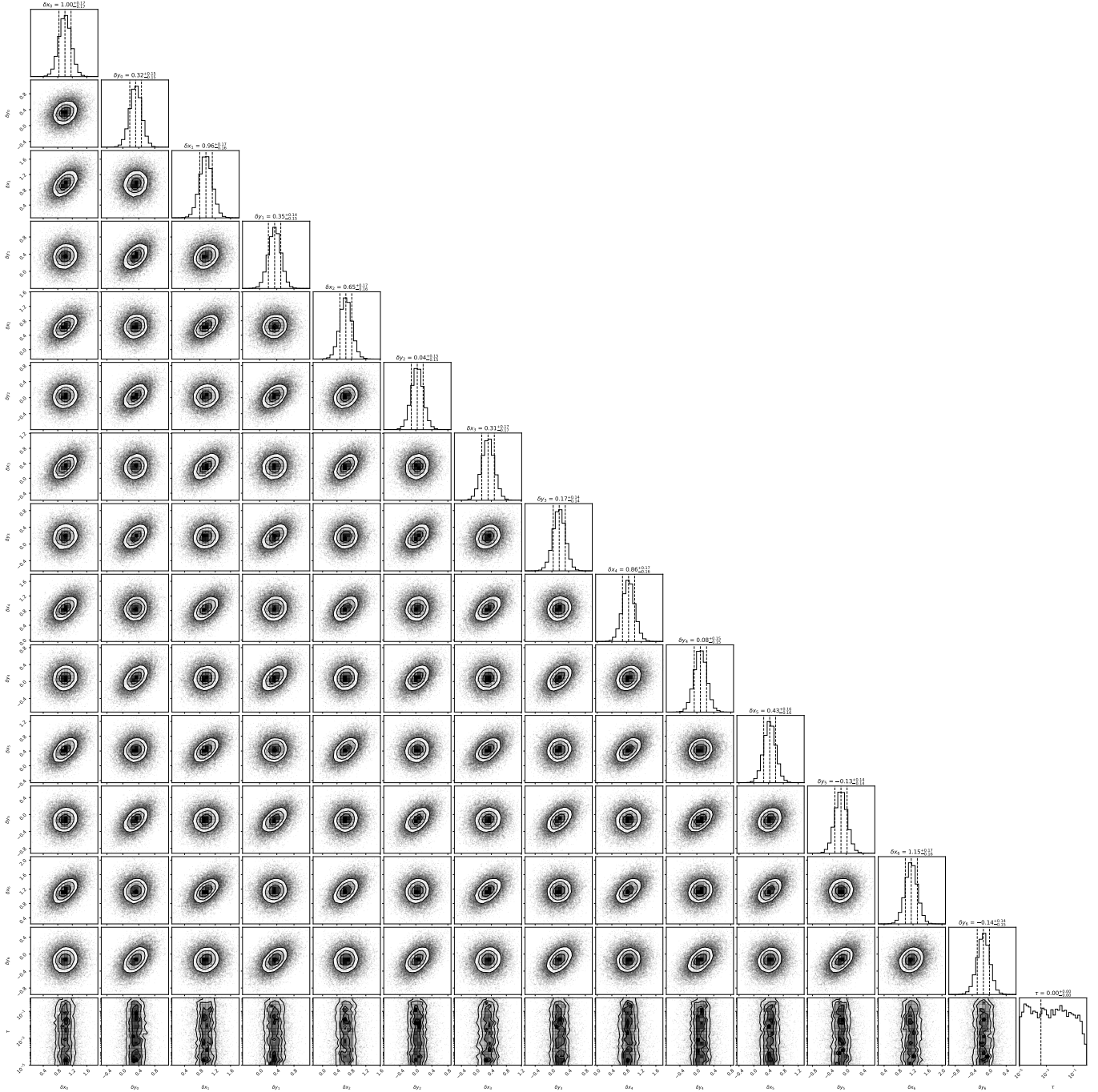


**Fig. 5.** Posterior distribution assuming common optical depth proportional to the disk brightness.

Description TODO.

tively. In the following we will use the most recent value of  $M_{disk} = 0.250 \pm 0.004 M_{\oplus}$ .

Assuming a uniform dust density  $\rho$  and grain radius  $r_{dust}$  in the disk, Wyatt (2008) writes the disk mass as

$$M_{disk} = 1.34\rho\bar{a}\sigma_{tot} \quad (15)$$

Using the values defined above I find

$$\rho = \frac{M_{disk}}{1.34\bar{a}\sigma_{tot}} = 1.5 \pm 0.025 \text{ g cm}^{-3} \quad (16)$$

This is larger than the value assumed in both Ricci et al. (2015) and van Sluijs et al. (2018) who both assume a uniform density of  $1.2 \text{ g cm}^{-3}$ , nevertheless it is within the expected range

for debris disks. As noted above, the estimated density is based on the previous work of Miyake & Nakagawa (1993) and Ricci et al. (2010). It should be noted that the stars (Taurus-Auriga star forming region), surveyed in these works were significantly younger than HD 107146 with ages of 0.1 Myr to 17 Myr. Still, Ricci et al. (2010) do not find an evolutionary trend of the spectral index  $\beta$  in their samples on which the estimations of the mean solid densities are based. Furthermore, it should also be noted that the dust masses for these disks are significantly higher than for the disk of HD 107146 (Ricci et al. 2010). While we avoid assuming the mean solid particle density we have used a somewhat arbitrary cut-off brightness at which the disk ends.

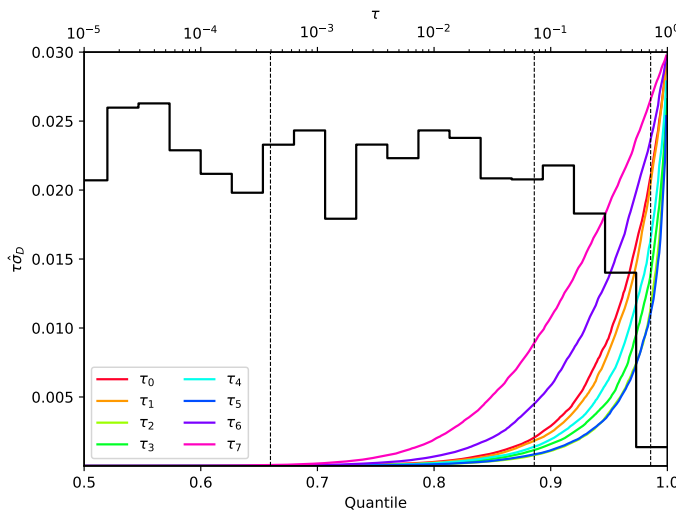


**Fig. 6.** Marginalized optical depth posterior distribution assuming common optical depth proportional to the disk brightness together with the inverse CDF without assuming proportionality scaled by the disk surface brightness.

## 7.2. Column Density

With above assumptions the column density  $\Sigma$  can be written as

$$\Sigma = \frac{\tau}{\sigma} m_p \quad \text{with} \quad \sigma = 2\pi a^2 \quad (17)$$

where  $\sigma$  is the effective cross section and  $m_p$  the mass of a particle (van Sluijs et al. 2018). Using Equation 13 the column density can be written explicitly as a function of the opacity and density.

$$\Sigma = \frac{2}{3} \tau \bar{a} \rho = 1.45 \times 10^{-7} \pm 2.44 \times 10^{-10} \text{ g cm}^{-2} \quad (18)$$

This upper limit is  $\sim 2$  orders of magnitude lower than the estimate by van Sluijs et al. (2018). This is almost completely due to the much lower opacity limit which we find in this work. This new value is, nevertheless, within the error of the previous work.

Mention, this is not a real difference, see fig, but instead do to the way we define the opacity, scaling it by the disk SB (arbitrary units). Reverting this scaling (see Figure 7) results in excellent agreement between our methods.

## 7.3. Opacity

From Equation 2 the opacity is related to the optical depth as:

$$\tau = \int \rho k dl \quad (19)$$

Assuming the vertical density profile can be assumed to fulfill  $\int \rho_l dl = \int \bar{\rho} dl$ , i.e. is well approximated by the average density we determined above we can write for the opacity of the debris disk:

$$\kappa = \frac{\tau}{\rho l} \quad (20)$$

From Hughes et al. (2018) we take the median ratio of disk height to radius  $l/r = 0.06$  which leads to an approximate disk height of HD 107146 of  $l \approx 14.4 \text{ AU}$  which implies a very dispersed disk at the radii we probe. From Equation 20 we then find an opacity of  $\kappa \approx 4.496 \times 10^{-22} \text{ cm}^2/\text{g}$ .

## 7.4. Comparison with Previous Work

From our analysis we find a optical depth much smaller than what could be detected by (van Sluijs et al. 2018) since our method has a higher accuracy. However, (Schneider et al. 2016) place a constraint based on assumption of the particle albedo  $\omega$  on the  $\omega\tau$  product. They find a  $(\omega\tau)_{max} = 5 \times 10^{-4}$  which would, with our results, imply an albedo of  $\lesssim 1$  which is bordering on being unphysical and disagrees with observations due to the particle temperature that dust with such an albedo would produce. However, since this is an estimation of the maximum albedo-optical-depth product this constraint is not necessarily incompatible with our work.

The review figure of the column depth of HD 107146s debris disk by van Sluijs et al. (2018), shown in Figure 7 cannot be used as a direct comparison with our results since other particle sizes are being probed by exploiting different mechanisms.

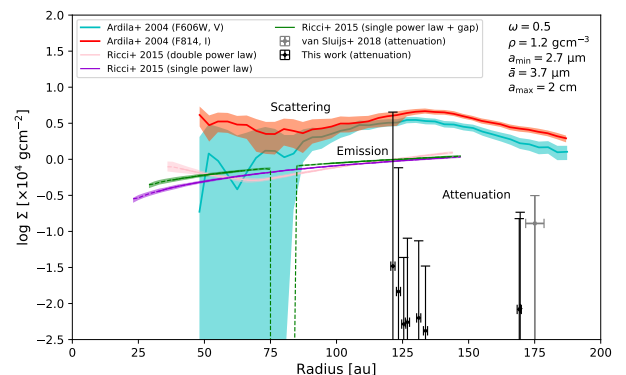


**Fig. 7.** Plot of the optical depths detected in the past for different mechanisms and particle sizes as well as the work of van Sluijs et al. (2018) and our estimate on  $\tau\hat{\sigma}_D$  with the upper limit for attenuation in the optical.

The optical depth we find is low for debris disks, especially ones with a high fractional luminosity, and is only 2 orders of magnitude above what a transport dominated disk would have (Krivov 2010).

From our initial assumption the optical depth varies over the disk proportional to its surface brightness.

## 8. Conclusion

Recently, the feasibility of differential photometry using light with a wavelength of  $\approx 5850 \text{ Å}$  for probing the optical depth through attenuation of a background galaxy has been shown for the debris disk of HD 107146. We use extinction of a transiting background galaxy to probe the optical depth of the debris disk of this solar analogue, which has in the past has been done at millimeter and optical wavelengths. However, in the past different mechanisms; emission and scattering, have been used.

Our result is near the estimated detection threshold of our method, with the upper limit of the optical depth  $\tau_{max} = 10^{-4} - 10^{-3}$ . This result is much lower than the previous upper limit, and agrees tenuously with independent estimates. Based on this result we also give some other, dependent estimations of disk parameters such as its density and opacity at the particle sizes probed.

Our work is important with respect to developing novel method for opacity estimations that is independent of some of the assumptions of previous methods. Furthermore, we also provide an independent constraint on the optical depth of a solar analogue which has been investigated for the presence of potential using indirect methods due to ring structures visible in its disk. The background galaxy will continue to transit the disk, and is at the time of writing behind its most dense part for particles of  $\mu\text{m}$ -sizes. New observations could find a lower limit on the opacity, especially when using better coronagraphs and detectors with higher signal-to-noise ratios. The method we use is not limited to the optical, instead it can be used at a wide range of wavelengths to probe different particle distributions in the disk.

*Acknowledgements.* Acknowledgements. – Observation campaign

## References

- Alexander, R., Pascucci, I., Andrews, S., Armitage, P., & Cieza, L. 2014, in Protostars and Planets VI, ed. V. Mannings, A. P. Boss, & S. S. Russell (Univ. of Arizona Press), pp. 475-496
- Ardila, D., Golicinski, D., Krist, J., et al. 2004, The Astrophysical Journal Letters, 617, L147
- Ardila, D., Golicinski, D., Krist, J., et al. 2005, The Astrophysical Journal, 624, L141
- Buchner, J. 2016, Statistics and Computing, 26, 383
- Buchner, J. 2019, PASP, 131, 108005
- Buchner, J. 2021, The Journal of Open Source Software, 6, 3001
- Chiang, E., Kite, E., Kalas, P., Graham, J., & Clampin, M. 2009, The Astrophysical Journal, 693, 734
- Dohnanyi, J. 1969, Journal of Geophysical Research, 74, 2531
- Draine, B. 2006, The Astrophysical Journal, 636, 1114
- Ertel, S., Wolf, S., Metchev, S., et al. 2011, Astronomy & Astrophysics, 533, A132
- Henyey, L. G. & Greenstein, J. L. 1941, Astrophysical Journal, vol. 93, p. 70-83 (1941), 93, 70
- Hughes, A. M., Duchêne, G., & Matthews, B. C. 2018, Annual Review of Astronomy and Astrophysics, 56, 541
- James, P. & Puxley, P. 1993, Nature, 363, 240
- Kenyon, S. J. & Bromley, B. C. 2005, The Astronomical Journal, 130, 269
- Krivov, A. V. 2010, Research in Astronomy and Astrophysics, 10, 383
- Marino, S., Carpenter, J., Wyatt, M., et al. 2018, Monthly Notices of the Royal Astronomical Society, 479, 5423
- Mesa, D., Marino, S., Bonavita, M., et al. 2021, Monthly Notices of the Royal Astronomical Society, 503, 1276
- Miyake, K. & Nakagawa, Y. 1993, icarus, 106, 20
- Moór, A., Ábrahám, P., Derekas, A., et al. 2006, The Astrophysical Journal, 644, 525
- Ricci, L., Carpenter, J., Fu, B., et al. 2015, The Astrophysical Journal, 798, 124
- Ricci, L., Testi, L., Natta, A., et al. 2010, Astronomy & Astrophysics, 512, A15
- Schneider, G., Debes, J. H., Grady, C. A., et al. 2018, The Astronomical Journal, 155, 77
- Schneider, G., Grady, C. A., Hines, D. C., et al. 2014, The Astronomical Journal, 148, 59
- Schneider, G., Hines, D. C., Holwerda, B. W., Kenworthy, M., & Stark, C. C. 2016, HST Proposal, 14714
- Schneider, G., Silverstone, M. D., Hines, D. C., et al. 2006, The Astrophysical Journal, 650, 414
- Stobie, E. & Ferro, A. 2006, in Astronomical Data Analysis Software and Systems XV, Vol. 351, 540
- Tanaka, H., Himeno, Y., & Ida, S. 2005, The Astrophysical Journal, 625, 414
- Tanaka, H., Inaba, S., & Nakazawa, K. 1996, Icarus, 123, 450
- van Sluijs, L., Vaenel, D., Holwerda, B. W., Kenworthy, M., & Schneider, G. 2018, Monthly Notices of the Royal Astronomical Society, 480, 914
- Weidenschilling, S. 1997, Icarus, 127, 290
- White, R. E. & Keel, W. C. 1992, Nature, 359, 129
- White III, R. E., Keel, W. C., & Conselice, C. J. 2000, The Astrophysical Journal, 542, 761
- Williams, J. P., Najita, J., Liu, M. C., et al. 2004, The Astrophysical Journal, 604, 414
- Wyatt, M. C. 2008, Annu. Rev. Astron. Astrophys., 46, 339